Check for updates

Role of electrostatic interactions in the adsorption of dye molecules by Ti₃C₂-MXenes†

Sehyeong Lim, Jin Hyung Kim, Hyunsu Park, Chaesu Kwak, Jeewon Yang, Jieun Kim, Seoung Young Ryu and Joohyung Lee [ID] *

MXenes, a new class of 2D materials, have recently attracted increasing attention as promising adsorbents for environmental remediation. It has been previously demonstrated that MXenes can successfully capture selected organic dyes from aqueous media; however, to date, the adsorption performance of MXenes for a wide variety of dyes in simulated real-life aquatic environments other than clean laboratory deionized (DI) water has not been systematically investigated. In this study, we systematically investigated the adsorption performance of delaminated Ti_3C_2-MXenes for six different organic dyes in aquatic media at different pH levels and ionic strengths. Our results strongly suggest the importance of the electrostatic interactions between the ionizable functional groups of MXenes and dyes for removal efficiency. The electrostatic repulsions between negatively charged MXenes and certain anionic dyes reduced the removal efficiencies of MXenes for these dyes in DI water; however, the presence of divalent cations significantly improved the removal efficiencies, possibly owing to the charge screening effects and like-charge attractions mediated by cation binding to the functionalities of dyes and MXenes. These results provide a rational strategy for optimizing the conditions for efficient removal of different types of organic dyes using MXenes.

1. Introduction

Water pollution, one of the most critical environmental issues that threaten ecosystems and humanity, is caused by contaminants such as organic matter and heavy metal ions, which dissolve in the water supply and industrial wastewater.[1,2] To date, different water treatment methods have been developed for removing contaminants and reusing purified water. Among these, adsorption is the most popular, owing to its high effectiveness, economic feasibility, and ease of operation.[3] Well-known examples of commercial adsorbents include activated carbons,[4] silicas,[5] and zeolites;[6] furthermore, new types of adsorbents are being actively developed.

Recently, transition metal carbides and/or nitrides ("MXenes"), a new class of 2D materials, have received increasing attention as adsorbents in environmental remediation applications.[7–9] MXenes are prepared *via* acid etching of the "A" elements from their $M_{n+1}AX_n$ ternary precursors (M: transition metal; A: Al, Si, Ga, *etc.*; X: C and/or N). This generates abundant surface functional sites, including hydroxyl (–OH) groups, which are suitable for adsorption applications.[10,11] Since Mashtalir *et al.*[12] first attempted to use titanium carbide (Ti_3C_2)-MXenes as

potential adsorbents for organic dyes, methylene blue (MB) and acid blue 80, as model aqueous pollutants, a number of studies have been performed employing pristine[13,14] or engineered MXenes as adsorbents.[15–17] Integration of the excellent adsorption properties of MXenes with their high aspect ratios, unique catalytic activity, and electronic conductivity has extended the environmental applications of MXenes in several areas such as membrane separation,[18] photocatalytic degradation,[19] and electrochemical sensing of different aqueous pollutants.[20]

The textile, paper, dye and dye intermediates, and pharmaceutical industries release more than 10 000 types of organic dyes in the environment.[21] These dyes are major aqueous pollutants and present persistent challenges for the water supply. Selected aqueous organic dyes have been successfully sequestrated by MXenes;[12,15,16] however, a study on the adsorption of a wider variety of dyes with different chemical structures has not been performed to date. Furthermore, previous studies only investigated the adsorptive performance of MXenes in clean laboratory deionized (DI) water instead of simulated real-life aquatic environments, which might be acid or alkaline and could contain salt ions.[22] The presence of salt ions in aquatic environments is of particular interest because MXenes present poor colloidal stability in natural or synthetic waters that contain mono- and/or divalent ions and present higher ionic strength than DI.[23,24] Such "mobility" problem could be successfully overcome by grafting salt-resistant polyelectrolytes on MXene surfaces;[24] however, insight into the adsorption properties of pristine MXenes in

Department of Chemical Engineering, Myongji University, 116 Myongji-ro, Cheoin-gu, Yongin, Gyeonggi-do, 17058, Korea. E-mail: ljbro@mju.ac.kr; Tel: +82-31-330-6386
† Electronic supplementary information (ESI) available: Zeta potential of MXenes measured in 0.5 M and 1 M NaCl solutions, removal of cationic dyes in 1 h batch adsorption experiments at different salinities. See DOI: 10.1039/d0ra10876f

saline environments would be extremely useful for designing MXene-based water treatment processes. In this study, we investigated the adsorption performance of delaminated Ti_3C_2-MXenes for six organic dyes in aquatic media with various pH levels and ionic strengths and discussed the adsorption mechanisms with a particular focus on the electrostatic interactions between the dyes and MXenes.

2. Materials and methods

2.1. Materials

Titanium aluminum carbide (Ti_3AlC_2, 98% purity) was purchased from American Elements (USA). Hydrochloric acid solution (HCl, >35%), sodium chloride (NaCl), calcium chloride dihydrate ($CaCl_2 \cdot 2H_2O$), and orange G (OG) were purchased from Daejung Co., Ltd. (Korea). Lithium fluoride (LiF, 98% purity) and lithium hydroxide monohydrate ($LiOH \cdot H_2O$) were purchased from Waco (Japan) and Duksan Co., Ltd. (Korea), respectively. MB, congo red (CR), and methyl red (MR) were purchased from Samchun Pure Chemical Co., Ltd. (Korea). Methyl violet (MV) and methyl orange (MO) were purchased from Junsei Chemical Co., Ltd. (Japan) and Showa Chemical Industry Co., Ltd. (Japan), respectively.

2.2. Preparation of delaminated Ti_3C_2-MXenes

0.8 g LiF was dissolved in 10 mL aqueous HCl solution (9 M) by magnetically stirring the mixture, into which 0.5 g Ti_3AlC_2 MAX phases were subsequently added. The entire mixture was magnetically stirred at RT for 24 h. The etched product was precipitated via centrifugation in a 50 mL conical tube and washed copiously with DI water until the measured pH of the supernatant became higher than 6. After the last washing step, the precipitated MXenes were redispersed in DI water and centrifugated at 3500 rpm for 2 min to discard the Ti_3AlC_2 residues and unsuccessfully delaminated MXenes. The concentration of the resulted aqueous MXene dispersion was determined gravimetrically by taking an aliquot of the sample and evaporating the water.

2.3. Batch adsorption experiments

For experiments in salt-free environments, each type of organic dye was individually dissolved in DI water to prepare stock solutions with a concentration of 75 mg L^{-1}. The pH of the stock solutions was adjusted to 2, 4, 6, 8, 10, or 12 using HCl and LiOH. For the adsorption experiments, 4 mL of stock dye solution with the desired pH was mixed with 2 mL of a MXene dispersion (2 mg mL^{-1}) in a 20 mL scintillation vial. The pH of the MXene dispersion was previously adjusted to match that of the dye solution. The resulting mixture, with initial dye and MXene concentrations of 50 mg L^{-1} and 0.67 mg mL^{-1}, respectively, was magnetically stirred at 700 rpm for 1 h. The product was centrifuged at 8000 rpm for 20 min to completely precipitate the adsorbent MXene, and the supernatant was filtered through a non-sterile polyethylene sulfone membrane with a pore size of 0.2 μm to remove the dusts before ultraviolet-visible (UV-vis) spectroscopy analysis.

For the experiments in salt-containing environments, each type of organic dye was dissolved in 0.006 M NaCl, 0.006 M $CaCl_2$, 0.015 M NaCl, or 0.015 M $CaCl_2$ solution to prepare stock solutions with dye concentrations of 75 mg L^{-1}. All tested dyes were completely soluble in the salt solutions at the given concentrations (except for CR; to be discussed below), as confirmed by observing no precipitants after centrifuging the solutions at 8000 rpm for 20 min. Similar to the experiments in salt-free environments, a 4 mL salt-containing stock dye solution and a 2 mL MXene dispersion (2 mg mL^{-1}) with matching pH were mixed in a 20 mL scintillation vial to obtain mixtures with initial dye and MXene concentrations of 50 mg L^{-1} and 0.67 mg mL^{-1}, respectively, in 0.004 M NaCl/$CaCl_2$ or 0.01 M NaCl/$CaCl_2$ solutions. The experimental procedure followed the same steps outlined for the salt-free environments.

For long-term adsorption experiments, the adsorption batches were scaled up to total mixture volumes of 180 mL, and the experiments were performed in 250 mL polypropylene bottles at a same magnetic stirring rate of 700 rpm for up to 96 h. Aliquots were collected at different times to determine the amount of dye adsorbed on MXenes.

2.4. Kinetic modeling

The time-dependent adsorption data of the long-term batch experiments were fit with several kinetic models to determine the adsorption mechanisms. The well-known pseudo-first order (PFO),[25] pseudo-second order (PSO),[26] and intra-particle diffusion (ID) models,[27] can be described using eqn (1), (2), and (3), respectively:

$$Q_t = Q_e(1 - e^{-k_1 t}) \tag{1}$$

$$Q_t = \frac{k_2 Q_e^2 t}{1 + k_2 Q_e t} \tag{2}$$

and

$$Q_t = k_p t^{0.5} + C \tag{3}$$

where Q_t (mg g^{-1}) and Q_e (mg g^{-1}) are the mass of adsorbed dye per mass of adsorbent at time t (h) and at equilibrium, respectively, k_1 (h^{-1}), k_2 (g (mg h)$^{-1}$), and k_p (mg (g h)$^{-1/2}$) are the rate constants for the respective models, and C is the intercept (mg g^{-1}).

2.5. Characterization

An EM-30AX (COXEM, Korea) table-top scanning electron microscopy (SEM) instrument was used to visualize the Ti_3AlC_2 MAX phase and Ti_3C_2-MXenes. A ZS90 (Malvern, UK) zetasizer was used to measure the zeta potential of the MXenes in salt-free and salt-containing aquatic media. A Mega-900 (SCINCO, Korea) UV-vis spectrometer was used to determine the concentration of residual organic dyes in the supernatants of the adsorption products. A K-Alpha$^+$ (Thermo Fischer Scientific, USA) X-ray photoelectron spectroscopy (XPS) apparatus and an AERIS (Malvern, UK) X-ray diffraction (XRD) device were used to characterize the Ti_3AlC_2 MAX phase and Ti_3C_2-MXenes before and after the adsorption experiments.

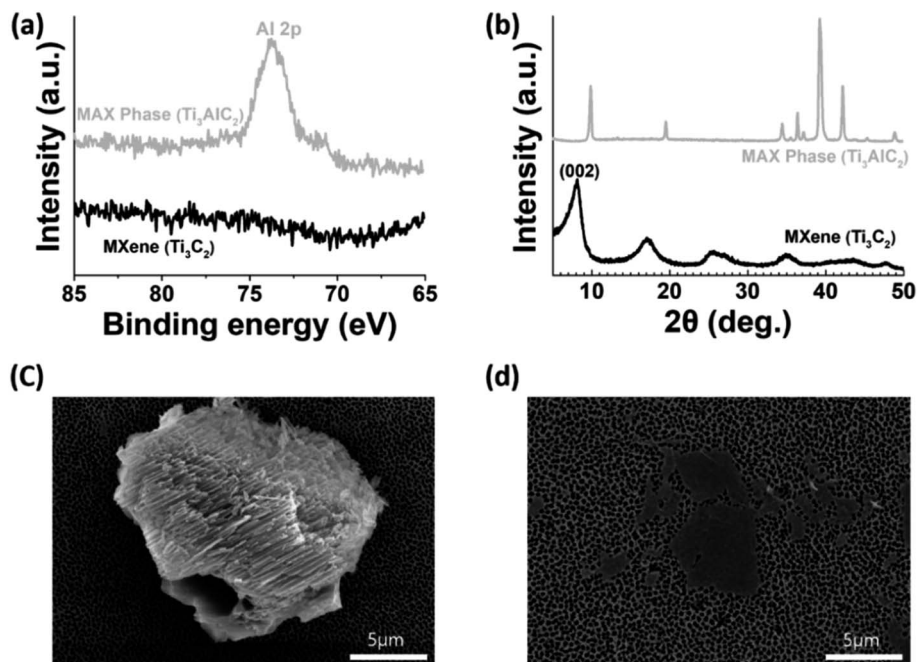**Fig. 1** (a) Al 2p XPS narrow scan profiles of Ti$_3$AlC$_2$ MAX phase (grey) and Ti$_3$C$_2$ MXene (black). (b) XRD patterns of Ti$_3$AlC$_2$ MAX phase (grey) and Ti$_3$C$_2$ MXene (black). SEM images of (c) unexfoliated Ti$_3$AlC$_2$ MAX phase and (d) delaminated Ti$_3$C$_2$ MXene (anodic alumina membranes were used as the substrate for the identification of thin MXene sheets).
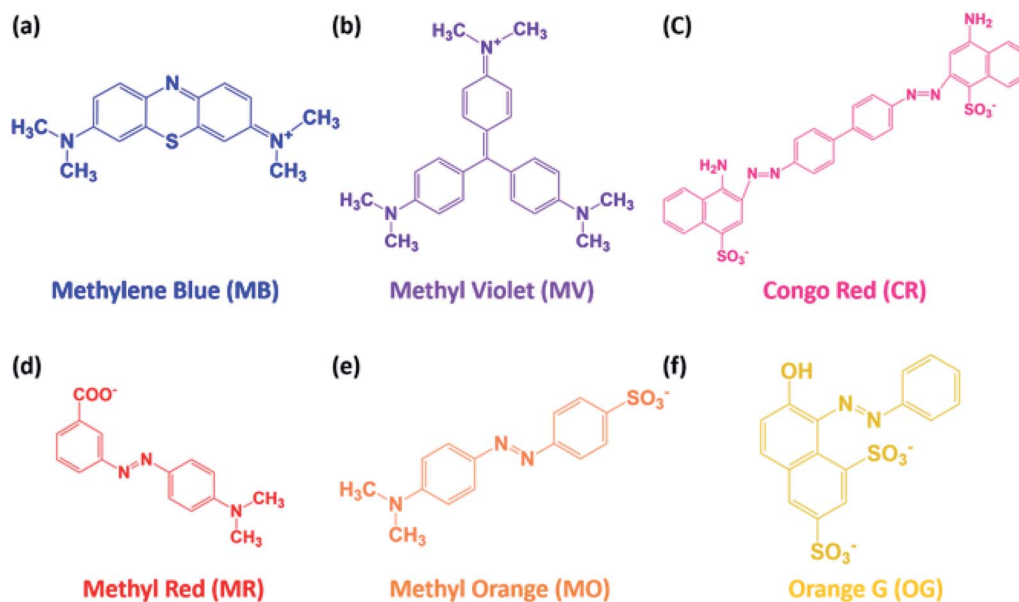

Fig. 2 Organic dyes used for batch adsorption experiments: (a) methylene blue (MB), (b) methyl violet (MV), (c) congo red (CR), (d) methyl red (MR), (e) methyl orange (MO), and orange G (OG).

3. Results and discussion

3.1. Effect of pH on the removal efficiency of MXenes for different aqueous organic dyes

Delaminated Ti$_3$C$_2$-MXenes were prepared by etching the Ti$_3$AlC$_2$ MAX phase using a LiF-containing concentrated HCl solution, following the literature.[10,11,24] The characteristic Al 2p peak at 73.61 eV of the precursor disappeared from the XPS profile of the etched product (Fig. 1a), which indicated that etching successfully removed the "A" layer from the MAX phase. The (002) peak in the XRD pattern of the etched product (Fig. 1b) was shifted toward lower 2θ values than that of the MAX phase, which suggested that the d-spacing increased, likely owing to the intercalation of Li$^+$ ions and introduction of

surface terminal groups, including –OH.[10] The SEM images of the precursor and etched product (Fig. 1c and d, respectively) revealed their 3D and 2D nature, respectively, and confirmed the successful delamination of Ti_3C_2-MXenes. MB, MV, CR, MR, MO, and OG dyes were used for the adsorption study, and their chemical structures are illustrated in Fig. 2.

To study the effect of the pH on the dye adsorption performance of MXenes, batch experiments were performed in aqueous dye solutions in the pH range of 2–12, at initial dye and MXene concentrations of 50 mg L^{-1} and 0.67 mg mL^{-1}, respectively (MB and MV were not analyzed at pH 12 because of dye discoloration[28] and precipitation). The removal efficiencies of the prepared MXenes for the dyes were evaluated by the calculated removal (%) defined as follows:

$$\text{Removal (\%)} = \left(\frac{C_0 - C_t}{C_0}\right) \times 100 (\%) \qquad (4)$$

where C_0 (mg L^{-1}) and C_t (mg L^{-1}) are the initial dye concentration and residual dye concentration at time t. The calculated removal (%) after 1 h are illustrated in Fig. 3.

Overall, the variation trends of the removal efficiencies *versus* pH was correlated with the charge type of organic dye. As the pH increased, the removal efficiencies of the cationic (MB and MV) and anionic dyes (CR, MR, MO, and OG) increased and decreased, respectively. The ever-present van der Waals interactions likely played a role in the adsorption of all dyes; however, the apparently opposite pH dependence of the removal efficiencies for cationic and anionic dyes suggested the importance of the electrostatic interactions between the dyes and MXenes, which should be related to the charging states of the interacting species.

Fig. 4 presents the measured zeta potentials of the prepared MXenes, which reflect the charging state of the MXene surfaces in the pH range of 2–12. The MXene surfaces were negatively charged over the entire investigated pH range, which was attributed to the deprotonated hydroxyl (–O^-) surface groups. This negative charging state of the MXene surfaces could promote the adsorption of cationic dyes *via* electrostatic attraction, particularly at high pH levels where the MXene surfaces were more negatively charged. At low pH levels, the MXene surfaces became relatively less negatively charged because of the neutralization of the –OH groups on their surface by the excess H^+ ions in solutions; consequently, the adsorption of cationic dyes could be less favored at low pH levels owing to the competition with excess H^+ ions. Thus, the higher (lower) negative surface charging of MXenes at higher (lower) pH explained the higher (lower) adsorption of cationic dyes in terms of the attractive electrostatic interactions.

Conversely, the repulsive electrostatic interactions would be dominant for the adsorption of anionic dyes, particularly at high pH levels at which the MXenes were more negatively charged, causing lower dye adsorption. The removal efficiencies of the MXenes for MR, MO, and OG were close to zero at pH levels above 8, 6, and 4, respectively, which indicated that the adsorption of these anionic dyes in these pH ranges was negligible (note that the adsorption of cationic dyes at lower pH levels, where the electrostatic attraction was expected to decrease, was still relatively high due to the van der Waals interactions in the absence of this electrostatic "barrier"). The removal efficiencies of the anionic dyes typically increased with decreasing pH. This was primarily attributed to the decrease in electrostatic repulsion as the anionic functionalities of the MXenes and dyes were gradually neutralized by the excess H^+ ions in the low pH region.

It is notable that the chemical structures of MR and MO were very similar except for their single anionic groups, *i.e.*,
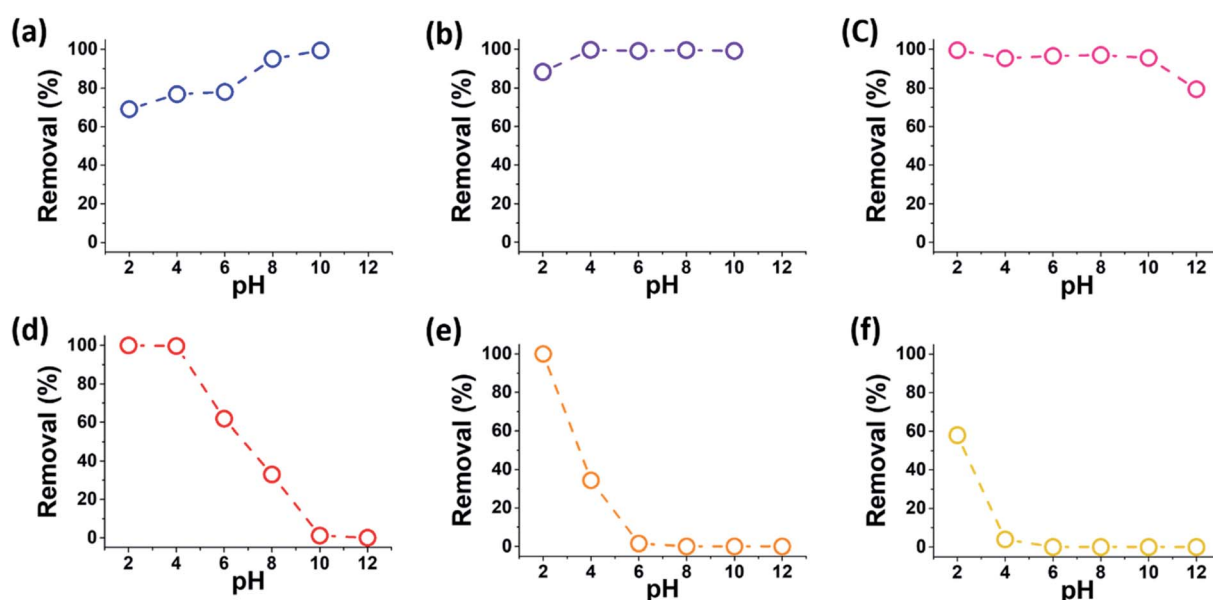

Fig. 3 Removal efficiencies of MXenes for (a) MB, (b) MV, (c) CR, (d) MR, (e) MO, and (f) OG in batch adsorption experiments performed at different pH levels for 1 h (C_0: 50 mg L^{-1} and MXene concentration: 0.67 mg mL^{-1}).
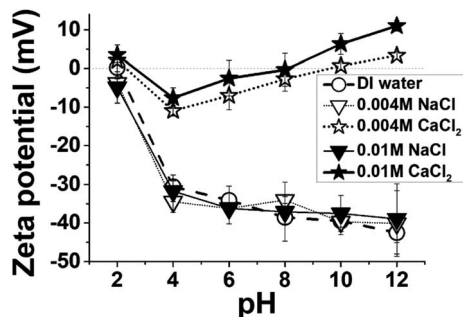
Fig. 4 Zeta potential of MXenes measured under different salinity conditions: DI water (empty circles), 0.004 and 0.01 M NaCl solutions (empty and solid inverse triangles, respectively), and 0.004 and 0.01 M CaCl₂ solutions (empty and solid stars, respectively).
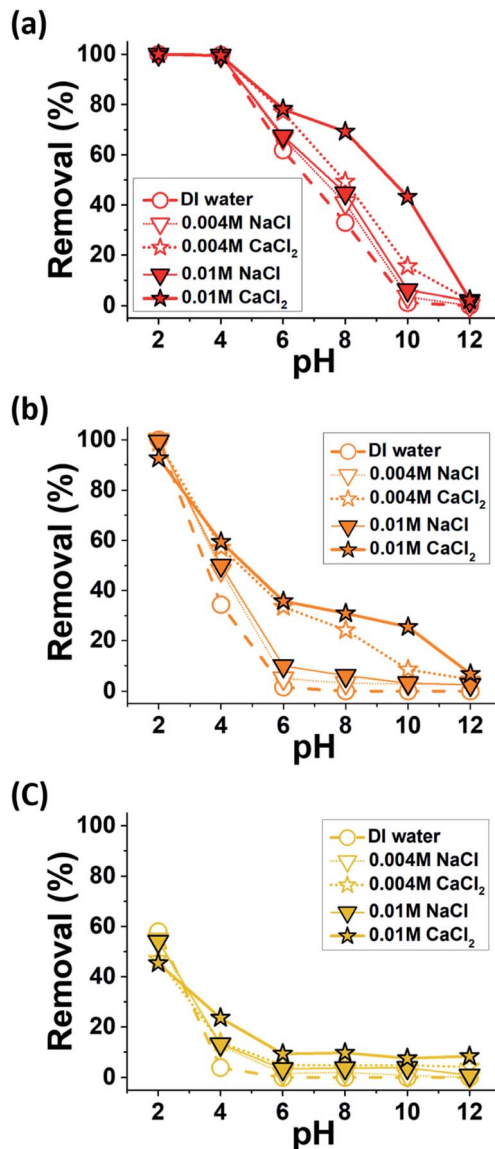

Fig. 5 Removal efficiencies of MXenes for (a) MR, (b) MO, and (c) OG anionic dyes in batch adsorption experiments performed at different salinities for 1 h (C_0: 50 mg L^{-1} and MXene concentration: 0.67 mg mL^{-1}).

carboxylic and sulfonic groups for MR and MO, respectively, yet the removal efficiency of the MXenes for MO was systematically lower than that for MR at pH ≤ 8. The difference in the removal efficiencies of the MXenes for MO and MR indicated the importance of the type of anionic functionality of the dye on the adsorption behavior when the repulsive electrostatic interactions with the negatively charged MXenes were dominant. It is more difficult to neutralize the strong sulfonic acid-derived anion of MO with excess H$^+$ ions at low pH than the weak carboxylic acid-derived anion of MR.[29,30] Therefore, it was highly probable that the electrostatic repulsion between MO and the MXene surface was stronger than that between MR and the MXene surface, which resulted in the adsorption of MO being lower than that of MR. Furthermore, the removal efficiency of OG, with two sulfonic groups, remained very low, owing to the strong repulsions between the two dye anions and negatively charged MXene surface over the entire pH range investigated except for pH 2. These results suggested that the very low adsorption of AB80 dyes, which also present two sulfonic groups, by MXenes, which has been previously reported by Mashtalir et al.,[12] might have been similarly affected by the strong dye-MXene electrostatic repulsions.

Interestingly, the removal efficiencies of MR, MO, and OG were remarkably high at pH 2, and were comparable to or even higher than those of the cationic dyes. It should be noted that the N atoms of the N=N bonds within the anionic azo dyes could be easily protonated at pH 2, as reported previously.[31–33] Hence, the protonated dye moieties could be electrostatically attracted to the anionic surface sites of the MXenes at this pH, whereas the anionic dye moieties were neutralized by the excess H$^+$ ions. Similarly, the typically high removal efficiencies of MXenes for anionic CR over the entire investigated pH range might be attributed to the two amine groups in the structure of CR, which could form ammonium cations with H$^+$ ions.[34] Still, the overall decrease in the removal efficiency of MXenes for CR with increasing pH matched those of other anionic dyes, owing to the electrostatic repulsions between CR and the negatively charged surface of MXenes.

Thus, the results of the batch adsorption experiments performed over a wide pH range strongly suggested the importance

of the electrostatic interactions between organic dyes and MXenes in the dye adsorption mechanisms.

3.2. Effects of salts

The effects of salt ions on the dye adsorption of MXenes were investigated under the same experimental conditions but with NaCl or CaCl₂, which are abundant in sea water and subsurface brines, deliberately added to the dye-contaminated solutions. We particularly focused on the anionic MR, MO, and OG, for which the removal efficiencies of the prepared MXenes in a salt-free environment over a wide pH range were unsatisfactory (Fig. 3). As illustrated in Fig. 5, the adsorption of these anionic dyes generally improved with increasing salt concentration (except for MO and OG at pH 2, which will be discussed further). In addition,

the improvement was more distinct when CaCl$_2$ was present in solutions than NaCl. The removal efficiencies of MXenes in CaCl$_2$ solutions were comparable to those of other adsorbents for MR,[35,36] MO,[37,38] and OG[39,40] reported in the literature.

The charge screening effect of the dissolved salt ions could contribute to the overall improvement in the adsorption of the anionic dyes by MXenes. The salt ions, which increased the ionic strength of the surrounding aqueous medium, reduced the thickness of the electrical double layer adjacent to the charged surfaces, or the Debye length (κ^{-1}),[41] which is defined as follows:

$$\kappa^{-1} = \frac{1}{\sqrt{\sum_i \dfrac{\rho_{\infty i} e^2 z_i^2}{\varepsilon \varepsilon_0 kT}}} \tag{5}$$

where $\rho_{\infty i}$ and z_i are the concentration and valence, respectively, of ion i in the bulk, e is the elementary charge, ε and ε_0 are the dielectric constant of the medium and vacuum permittivity, respectively, k is the Boltzmann constant, and T is the temperature. At a small κ^{-1}, the long-range electrostatic repulsions between dyes and the MXene surface could be effectively suppressed. This would allow for a closer approach of the like-charged entities, which should lead to an increase in adsorption. The order of magnitude of the calculated κ^{-1} values for the four tested salt solutions matched the relative dye removal efficiencies of MXenes in those solutions (Table 1).

The like-charge attractions[42,43] mediated by the binding of divalent Ca^{2+} ions to the anionic functional groups of the MXenes and dyes could significantly contribute to the improved dye removal efficiencies of MXenes. It has been reported by a number of studies that Ca^{2+} ions could irreversibly adsorb onto the anionic sites of various chemical compounds, such as carboxylates and sulfonates, in aqueous media.[22,24,30,44–46] When a divalent Ca^{2+} cation binds to a monovalent anionic site, a local charge inversion[47,48] could occur at the adsorption site and the net charge changes from (−1) to (+1), which could subsequently attract another anionic species. For MXenes, the intercalation of Ca^{2+} ions into multi-layered MXenes has been reported by the previous literature,[18,49] where the binding of Ca^{2+} ions to the anionic sites of two adjacent MXene layers sometimes resulted in changes in the interlayer distance. However, to the best of our knowledge, the binding of Ca^{2+} ions to the colloidal surfaces of delaminated MXenes and its electrostatic effects have not been reported to date. The zeta potentials of MXenes in CaCl$_2$ solutions were significantly lower than those in DI water and NaCl solutions, and at some pH levels, the sign of measured zeta potential was inverted to the positive (Fig. 4). This was

attributed to the Ca^{2+} binding to the anionic functionalities of MXenes, likely the –O$^-$ groups. The significant decrease in magnitude of the negative zeta potential of MXenes in CaCl$_2$ solutions should not be exclusively attributed to the charge screening effects, because the MXenes still maintained high negative zeta potential values in the 0.05 M and 0.1 M NaCl solutions, and their κ^{-1} values were 1.36 and 0.96 nm, respectively (Fig. S1, ESI†). Owing to the numerous effective surface cationic sites produced on the surfaces of MXenes *via* Ca^{2+} binding, the adsorption of anionic dyes could occur more easily in CaCl$_2$ solutions than in NaCl solutions as well as in the salt-free water, and this was consistent with the results presented in Fig. 5. We hypothesized that Ca^{2+} ions could also bind to the interlayer anionic sites of some incompletely delaminated MXenes, which promoted the intercalation of dye molecules. This will be discussed in more detail in the next section.
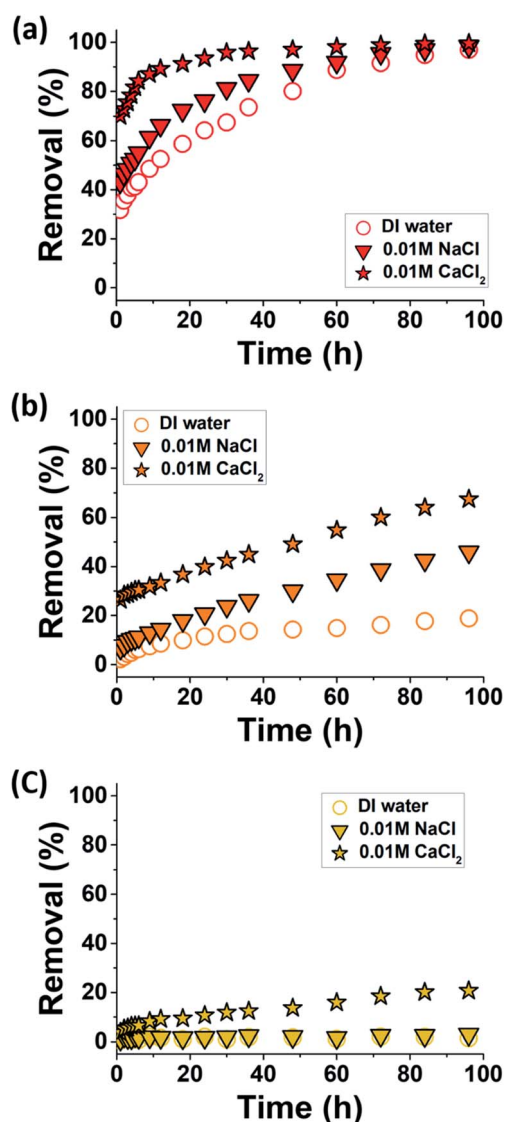

Fig. 6 Time-dependent removal efficiencies of MXenes for (a) MR, (b) MO, and (c) OG anionic dyes in batch adsorption experiments performed at different salinities for up to 96 h (C_0: 50 mg L^{-1} and MXene concentration: 0.67 mg mL^{-1}).

Table 1 Calculated Debye length (κ^{-1}) for the four tested salt solutions

Salt solution	κ^{-1} (nm)
0.004 M NaCl	4.81
0.01 M NaCl	3.04
0.004 M CaCl$_2$	2.78
0.01 M CaCl$_2$	1.76

This hypothetical adsorption mechanism involving Ca^{2+} ion binding could explain the observed dye specificity with respect to the removal efficiencies of MXenes in $CaCl_2$ solutions, which was most noticeable at pH 10, where the removal efficiencies of MXenes for all the dyes in DI water were practically zero. The increase in the removal efficiency of MXenes for MR was significantly higher than that for MO in $CaCl_2$ solutions with identical ionic strengths, despite the highly similar chemical structures of MR and MO. This might be attributed to the carboxyl group of MR being more susceptible to Ca^{2+} ions binding than the sulfonic group of MO.[29,30] The removal efficiency of OG from a $CaCl_2$ solution with the same concentration was the lowest because OG presented two sulfonic groups with low Ca^{2+} binding affinity. Dye specificity was not distinct at the highest pH of 12, probably because Ca^{2+} ions formed calcium hydroxide with the excess OH^- ions. Interestingly, the salts presented little effect or even decreased dye adsorption at the lowest pH of 2. The decrease in dye adsorption at pH 2 was more noticeable for the $CaCl_2$ solutions and might be attributed to the electrostatic repulsions between the protonated dyes (discussed in the previous section) and Ca^{2+}-bound MXenes, which presented net positive charges at this low pH.

Another possible mechanism for the improved dye removal efficiencies of MXenes in the presence of salts might be the salting-out effect,[50] that is, the decrease in solubility and precipitation of dyes at high salt concentrations. This effect was closely related to the aforementioned binding of ions to dyes, which could result in the local dehydration[22,30,46] of the charged moieties of dyes dissolved in aqueous media. The adsorption of such hydrophobized dyes onto the available colloidal surface sites would be entropically more favored than that of the fully dissociated dyes in the salt-free water. For CR-contaminated solutions, immediate precipitation of dyes was observed with the addition of $CaCl_2$, even in the absence of MXenes, which demonstrated the salting-out effect (adsorption experiments were not performed).

The overall results strongly suggested the importance of salt ion–MXene and salt ion–dye interactions and the decrease in electrical double layer thickness caused by mobile salt ions for the improved adsorptive removal of anionic dyes by MXenes in saline solutions. Electrostatic attractions predominated the interactions of MB and MV with MXenes in salt-free environments, and consequently, the salts presented minor effects on the overall removal efficiencies of MXenes for these dyes. This might be attributed to the weakening of the electrostatic attractions between dyes and MXenes, which decreased removal efficiencies, being offset by the salting-out effect, which increased removal efficiencies. The removal efficiencies of MXenes for MB and MV in salt solutions remained as high as those in the salt-free environments (Fig. S2, ESI†).

3.3. Effect of contact time

To investigate the effect of contact time on the removal efficiencies of MXenes for the MR, MO, and OG anionic dyes, batch adsorption experiments were performed at pH 8 under the same experimental conditions mentioned in the previous section but for extended periods of up to 96 h, and the results are illustrated in Fig. 6.

With increasing contact time, dye removal gradually increased for all anionic dyes, except for OG in DI water and 0.01 M NaCl solution, for which the most significant
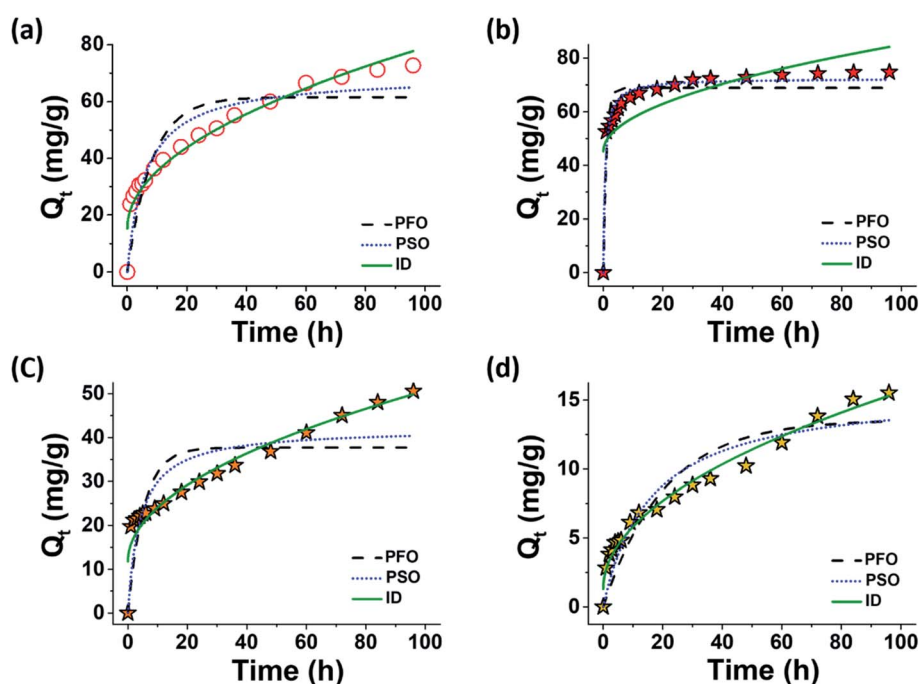

Fig. 7 Kinetic model fitting of some selected time-dependent dye adsorption data: (a) MR in DI water, (b) MR in a 0.01 M $CaCl_2$ solution, (c) MO in a 0.01 M $CaCl_2$ solution, and (d) OG in 0.01 M $CaCl_2$ solution.

Table 2 Parameters extracted from the kinetic model fitting of all data sets

Model	Parameter	MR			MO			OG		
		DI water	0.01 M NaCl	0.01 M CaCl$_2$	DI water	0.01 M NaCl	0.01 M CaCl$_2$	DI water	0.01 M NaCl	0.01 M CaCl$_2$
PFO	Q_e (mg g^{-1})	61.5646	64.1478	68.9024	12.2897	33.6508	37.7155	1.1527	1.5262	13.5683
	k_1 (h^{-1})	0.1225	0.2218	0.9649	0.0610	0.0287	0.1893	0.5456	0.9532	0.0488
	R^2	0.7874	0.7982	0.8927	0.9453	0.9252	0.601	0.4762	0.5716	0.8308
PSO	Q_e (mg g^{-1})	69.2133	69.6761	72.2903	14.7035	43.4233	42.0975	1.2225	1.6099	15.7833
	k_2 (g (mg h)$^{-1}$)	0.0023	0.0046	0.0228	0.0046	0.0006	0.0058	0.7082	0.9142	0.0039
	R^2	0.8849	0.9046	0.9697	0.9764	0.9417	0.7475	0.4883	0.5932	0.8871
ID	k_p mg (g h)$^{-1/2}$	6.3752	5.8562	3.9739	1.3899	3.3372	3.8885	0.0774	0.1086	1.4311
	C (mg g^{-1})	15.2931	24.3277	45.1883	0.9884	0.2941	11.7851	0.6582	0.9043	1.2885
	R^2	0.9497	0.8547	0.4471	0.9781	0.9919	0.9142	0.2449	0.4065	0.9817

electrostatic dye–MXene repulsions were expected. The removal rates of the anionic dyes followed the same overall trends observed after 1 h of adsorption, namely MR > MO > OG (Fig. 3 and 5). The removal rate of MR was the highest, and approximately 100% removal was reached before the end of the experiments (Fig. 6a). Furthermore, among the three tested aqueous media (*i.e.*, DI water, 0.01 M NaCl, and 0.01 M CaCl$_2$), the removal rate was the highest in the CaCl$_2$ solution and the lowest in DI water (Fig. 6a).

Kinetic model fitting of the time-dependent MR adsorption was performed, and the results are illustrated in Fig. 7a and b (DI water and 0.01 M CaCl$_2$, respectively) and are summarized in Table 2 (DI water, 0.01 M NaCl, and 0.01 M CaCl$_2$). The PFO and PSO models poorly fit the data in DI water (Fig. 7a), which indicated that the MR adsorption mechanism in this medium was not simply a consequence of the kinetic collisions between adsorbates and the unoccupied sites on the adsorbent surface. This somewhat reflected the repulsive nature of the anionic dye–MXene interactions in salt-free environments, which could prevent the collisions between the interacting species. Conversely, the fitting of the same data with the ID model yielded an excellent result. This indicated that the MR adsorption in DI water might be mainly driven by intra-particle diffusion.[13] For MXenes, this likely involved the diffusion of MR into the interlayer spaces of a few incompletely delaminated MXene

sheets, which was, in part, a thermodynamically driven process.[51]

The ID model poorly fit the data in the 0.01 M CaCl$_2$ solution (Fig. 7b). The high y-intercept value of the fit equation (C in Table 2) suggested that mechanisms other than ID were involved in the adsorption process. The PSO model fit the experimental results for the adsorption in the 0.01 M CaCl$_2$ solution the best, unlike the data for the adsorption in DI water. This suggested that the adsorption might have been the consequence of the collisions between the anionic dyes and surface sites of MXenes, which, according to our hypothesis, could be promoted *via* Ca^{2+} ion binding to the anionic groups of the interacting species. It should be noted that these phenomenological modeling results do not necessarily exclude the possibility of the intra-particle diffusion (which will be discussed further, below). We hypothesized that the intra-particle diffusion could still occur, while the dye adsorption at the external surface sites was significantly increased owing to the support of the adsorbed Ca^{2+} ions at the same time.

The removal efficiencies of MXenes for MO and OG did not reach equilibrium values until the end of the experiment (96 h), which indicated that the adsorption of these sulfonated dyes on the MXene surfaces was a very slow process. The time-dependent adsorption data for MO and OG in 0.01 M CaCl$_2$ solutions were best fit with the ID model, whereas the other two models completely failed to reproduce these data sets (Fig. 7c and d). This implied that, similar to the cases of MR in DI water, the adsorption behaviors of MO and OG in 0.01 M CaCl$_2$ solutions were not a simple consequence of the kinetic collisions between adsorbates and the unoccupied sites on the adsorbent surface, and this was attributed to the low binding affinity of the sulfonated dyes on the Ca^{2+}-bound MXene surfaces.
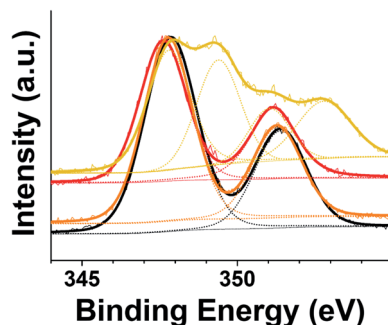

Fig. 8 Ca 2p XPS narrow scan profiles and curve-fitting and deconvolution results for the precipitants of four samples: {MXenes, Ca^{2+}} (black), {MXenes, Ca^{2+}, MR} (red), {MXenes, Ca^{2+}, MO} (orange), and {MXenes, Ca^{2+}, OG} (dark yellow).

Table 3 XPS binding energies of the most intense Ca 2p$_{3/2}$ peaks

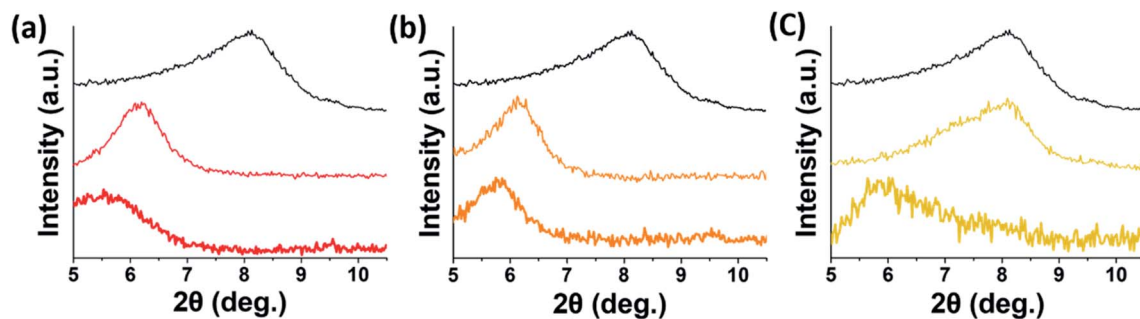| Sample precipitants	Ca 2p$_{3/2}$ binding energy
{MXenes, Ca^{2+}}	347.86 eV
{MXenes, Ca^{2+}, MR}	347.61 eV
{MXenes, Ca^{2+}, MO}	347.77 eV
{MXenes, Ca^{2+}, OG}	347.80 V

Fig. 9 XRD patterns of the precipitants of pristine MXenes (before adsorption, black) and samples collected after 96 h of adsorption experiments for (a) MR, (b) MO, and (c) OG under different conditions: DI water (thin line) and 0.01 M CaCl$_2$ solution (thick line).

XPS analyses were performed for the precipitated adsorbents after 96 h. The normalized narrow scan profile for the characteristic Ca 2p peaks and the binding energies for the most intense Ca 2p$_{3/2}$ deconvolution peaks are illustrated in Fig. 8 and Table 3, respectively. The low shift of the Ca 2p$_{3/2}$ peak from that of {MXenes, Ca^{2+}} (347.86 eV) was the most significant for the {MXenes, Ca^{2+}, MR} sample (347.61 eV), followed by {MXenes, Ca^{2+}, MO} (347.77 eV) and {MXene, Ca^{2+}, OG} (347.80 eV). This indicated that the adsorption of the MR dye on Ca^{2+}-bound MXene surfaces was likely the highest among the three anionic dyes, which was consistent with the results of long-term adsorption experiments and modeling analysis.

Whereas the XPS analysis revealed the adsorption characteristics of different dyes on the external surfaces of MXenes, the XRD spectra illustrated the significance of intra-particle diffusion or intercalation of dyes into incompletely delaminated MXene sheets, based on the degree of low shift of the peak associated with the (002) basal plane of MXenes. The (002) peaks of the precipitated adsorbents of all dyes in the 0.01 M CaCl$_2$ solution occurred at much lower 2θ angles than those in the salt-free environment (Fig. 9). This indicated that the interlayer spacings of the non-delaminated MXenes were much larger in the 0.01 M CaCl$_2$ solution than in DI water, and the removal of dyes *via* intercalation was more efficient in the 0.01 M CaCl$_2$ solution than in DI water. In addition, the interlayer distance was the largest for the {MXenes, Ca^{2+}, MR} sample (15.97 Å), followed by {MXenes, Ca^{2+}, MO} (15.38 Å) and {MXene, Ca^{2+}, OG} (14.72 Å), which was consistent with the final removal efficiencies of MXenes for these dyes.

Thus, the results of XPS and XRD analyses suggested that the removal of anionic dyes by MXenes could be improved *via* adsorption on the external MXene surfaces and intercalation in the presence of Ca^{2+} ions.

4.   Conclusion

In this study, the adsorption performance of delaminated Ti$_3$C$_2$-MXenes for six organic dyes: MB, MV, CR, MR, MO, and OG, was systematically investigated in aqueous media with different pH levels and ionic strengths. The adsorption of dyes on MXenes was significantly affected by the electrostatic dye–MXene interactions. For the cationic dyes, the electrostatic attractions between the dye cations and negatively charged MXenes were

dominant, and the removal efficiencies of MXenes for the dyes increased at high pH levels, where MXenes were more negatively charged. For the anionic dyes, electrostatic repulsions were dominant, and the pH dependence of the dye removal efficiencies was the opposite of that for the cationic dyes. Owing to the electrostatic repulsions, the removal efficiencies of MXenes for the anionic dyes, except for CR, which presented two protonatable amine groups in addition to the anionic groups, were generally low in a wide range of pH; however, the presence of salt ions, particularly the divalent Ca^{2+}, could significantly increase removal efficiencies *via* charge screening effects and specific binding to the functionalities of the dyes and MXenes. Correlative investigations using XPS, XRD, and kinetic modeling provided an in-depth mechanistic picture of the salt-mediated increase in the removal efficiencies of MXenes for anionic dyes, which suggested that both external and interlayer adsorption processes might be important. This is the first report on the use of negatively charged colloidal MXenes as adsorbents in aqueous media in a wide pH range for cationic dyes, for which the favorable adsorption was somewhat trivial, and also for anionic dyes, with functional groups such as carboxylates and sulfonates, which are susceptible to salt ion binding. It should be noted that the pristine MXenes were not subjected to physicochemical modification; moreover, external energy sources, such as UV light, have not been used to improve the removal efficiencies of MXenes for anionic dyes. Therefore, it is expected that MXenes could remove other dyes with similar functionalities from real-life environments,[23] including groundwater, which typically contains salt ions, more efficiently than from laboratory DI water. In this regard, sea water or subsurface brine with high salinities might be considered useful working solvents for the removal of mixtures of different cationic and anionic dyes using MXenes as adsorbents. The results of this study are expected to be very useful for predicting the removal efficiencies of MXenes for organic dyes and similar contaminants in arbitrary aquatic environments and determining the optimal process conditions for successful water treatment. Furthermore, the improved dye adsorption achieved *via* the simple addition of salt ions, without modifying the pristine MXenes or using external energy sources, which might degrade the original materials, could present potential implications in several energy applications, including the development of dye-sensitized solar cells.[52]

Conflicts of interest

There are no conflicts to declare.

Acknowledgements

References

1 R. P. Schwarzenbach, T. Egli, T. B. Hofstetter, U. Von Gunten and B. Wehrli, *Annu. Rev. Environ. Resour.*, 2010, **35**, 109–136.

2 P. K. Goel, *Water Pollution: Causes, Effects and Control*. 2006.

3 S. De Gisi, G. Lofrano, M. Grassi and M. Notarnicola, Characteristics and adsorption capacities of low-cost sorbents for wastewater treatment: A review, *Sustainable Mater. Technol.*, 2016, **9**, 10–40.

4 X. M. Ren, J. X. Li, X. L. Tan and X. K. Wang, Comparative Study of Graphene Oxide, Activated Carbon and Carbon Nanotubes as Adsorbents for Copper Decontamination, *Dalton Trans.*, 2013, **42**, 5266–5274.

5 Q. Huang, M. Liu, L. Mao, D. Xu, G. Zeng, H. Huang, R. Jiang, F. Deng, X. Zhang and Y. Wei, Surface Functionalized SiO_2 Nanoparticles with Cationic Polymers *via* the Combination of Mussel Inspired Chemistry and Surface Initiated Atom Transfer Radical Polymerization: Characterization and Enhanced Removal of Organic Dye, *J. Colloid Interface Sci.*, 2017, **499**, 170–179.

6 S. A. Kim, S. K. Kannan, K. J. Lee, Y. J. Park, P. J. Shea, W. H. Lee, H. M. Kim and B. T. Oh, Removal of Pb(II) from Aqueous Solution by a Zeolite–Nanoscale Zero-Valent Iron Composite, *Chem. Eng. J.*, 2013, **217**, 54–60.

7 K. Rasool, R. P. Pandey, P. A. Rasheed, S. Buczek, Y. Gogotsi and K. A. Mahmoud, Water Treatment and Environmental Remediation Applications of Two-Dimensional Metal Carbides (MXenes), *Mater. Today*, 2019, **30**, 80–102.

8 Y. Zhang, L. Wang, N. Zhang and Z. Zhou, Adsorptive Environmental Applications of MXene Nanomaterials: A Review, *RSC Adv.*, 2018, **8**, 19895–19905.

9 J. Chen, Q. Huang, H. Huang, L. Mao, M. Liu, X. Zhang and Y. Wei, Recent Progress and Advances in the Environmental Applications of MXene Related Materials, *Nanoscale*, 2020, **12**, 3574–3592.

10 M. Alhabeb, K. Maleski, B. Anasori, P. Lelyukh, L. Clark, S. Sin and Y. Gogotsi, Guidelines for Synthesis and Processing of Two-Dimensional Titanium Carbide (Ti3C2Tx MXene), *Chem. Mater.*, 2017, **29**, 7633–7644.

11 S. Lim, H. Park, J. Yang, C. Kwak and J. Lee, Stable Colloidal Dispersion of Octylated Ti3C2-MXenes in a Nonpolar Solvent, *Colloids Surf., A*, 2019, **579**, 123648.

12 O. Mashtalir, K. M. Cook, V. N. Mochalin, M. Crowe, M. W. Barsoum and Y. Gogotsi, Dye Adsorption and Decomposition on Two-Dimensional Titanium Carbide in Aqueous Media, *J. Mater. Chem. A*, 2014, **2**, 14334–14338.

13 A. Shahzad, K. Rasool, W. Miran, M. Nawaz, J. Jang, K. Mahmoud and D. S. Lee, Two-Dimensional Ti3C2Tx MXene Nanosheets for Efficient Copper Removal from Water, *ACS Sustainable Chem. Eng.*, 2017, **5**, 11481–11488.

14 Y. Ying, Y. Liu, X. Wang, Y. Mao, W. Cao, P. Hu and X. Peng, Two-Dimensional Titanium Carbide for Efficiently Reductive Removal of Highly Toxic Chromium(VI) from Water, *ACS Appl. Mater. Interfaces*, 2015, **7**, 1795–1803.

15 W. Zheng, P. Zhang, W. Tian, X. Qin, Y. Zhang and Z. M. Sun, Alkali treated Ti3C2Tx MXenes and Their Dye Adsorption Performance, *Mater. Chem. Phys.*, 2018, **206**, 270–276.

16 Y. Lei, Y. Cui, Q. Huang, J. Dou, D. Gan, F. Deng, M. Liu, X. Li, X. Zhang and Y. Wei, Facile Preparation of Sulfonic Groups Functionalized MXenes for Efficient Removal of Methylene Blue, *Ceram. Int.*, 2019, **45**, 17653––17661.

17 D. Gan, Q. Huang, J. Dou, H. Huang, J. Chen, M. Liu, Y. Wen, Z. Yang, X. Zhang and Y. Wei, Bioinspired Functionalization of MXenes (Ti3C2Tx) with Amino Acids for Efficient Removal of Heavy Metal Ions, *Appl. Surf. Sci.*, 2020, **504**, 144603.

18 C. E. Ren, K. B. Hatzell, M. Alhabeb, Z. Ling, K. A. Mahmoud and Y. Gogotsi, Charge- and Size-Selective Ion Sieving Through Ti3C2Tx MXene Membranes, *J. Phys. Chem. Lett.*, 2015, **6**, 4026–4031.

19 C. Peng, X. Yang, Y. Li, H. Yu, H. Wang and F. Peng, Hybrids of Two-Dimensional Ti3C2 and TiO2 Exposing {001} Facets toward Enhanced Photocatalytic Activity, *ACS Appl. Mater. Interfaces*, 2016, **8**, 6051–6060.

20 E. Lee, A. VahidMohammadi, B. C. Prorok, Y. S. Yoon, M. Beidaghi and D.-J. Kim, Room Temperature Gas Sensing of Two-Dimensional Titanium Carbide (MXene), *ACS Appl. Mater. Interfaces*, 2017, **9**, 37184–37190.

21 Z. Carmen and S. Daniel, Textile Organic Dyes – Characteristics, Polluting Effects and Separation/Elimination Procedures from Industrial Effluents – A Critical Overview, in *Organic Pollutants Ten Years After the Stockholm Convention - Environmental and Analytical Update*, 2012. pp. 55–86.

22 H. Park, S. Lim, J. Yang, C. Kwak, J. Kim, J. Kim, S. S. Choi, C. B. Kim and J. Lee, A Systematic Investigation on the Properties of Silica Nanoparticles "Multipoint"-Grafted with Poly(2-acrylamido-2-methylpropanesulfonate-co-acrylic Acid) in Extreme Salinity Brines and Brine-Oil Interfaces, *Langmuir*, 2020, **36**, 3174–3183.

23 Y. Xie, Y. Gao, X. Ren, G. Song, A. Alsaedi, T. Hayat and C. Chen, Colloidal Behaviors of Two-Dimensional Titanium Carbide in Natural Surface Waters: The Role of Solution Chemistry, *Environ. Sci. Technol.*, 2020, **54**, 3353–3362.

24 S. Lim, H. Park, J. Kim, J. Yang, C. Kwak, J. Kim, S. Ryu and J. Lee, Polyelectrolyte-grafted Ti3C2-MXenes stable in extreme salinity aquatic conditions for remediation of contaminated subsurface environments, *RSC Adv.*, 2020, **10**, 25966–25978.

25 S. Lagergren, Zur theorie der sogenannten adsorption gelöster stoffe, *K. Sven. Vetenskapsakad. Handl.*, 1898, **24**, 1–39.

26 Y. S. Ho and G. McKay, Pseudo-second order model for sorption processes, *Process Biochem.*, 1999, **34**, 451–465.

27 F. C. Wu, R. L. Tseng and R. S. Juang, Initial behavior of intraparticle diffusion model used in the description of adsorption kinetics, *Chem. Eng. J.*, 2009, **153**, 1–8.

28 L. Dayo Felix, Kinetic Study of the Discoloration of Crystal Violet Dye in Sodium Hydroxide Medium, *J. Chem. Appl. Chem. Eng.*, 2018, **2**, 1000115.

29 J. K. Newman and C. L. McCormick, Water-Soluble Copolymers. 52. Sodium-23 NMR Studies of Ion-Binding to Anionic Polyelectrolytes: Poly(sodium 2-acrylamido-2-methylpropanesulfonate), Poly- (sodium 3-acrylamido-3-methylbutanoate), Poly(sodium acrylate), and Poly(sodium galacturonate), *Macromolecules*, 1994, **27**, 5114–5122.

30 J. Lee, E. Moesari, C. B. Dandamudi, G. Beniah, B. Chang, M. Iqbal, Y. Fei, N. Zhou, C. J. Ellison and K. P. Johnston, Behavior of Spherical Poly(2-acrylamido-2-methylpropanesulfonate) Polyelectrolyte Brushes on Silica Nanoparticles up to Extreme Salinity with Weak Divalent Cation Binding at Ambient and High Temperature, *Macromolecules*, 2017, **50**, 7699–7711.

31 S. K. Park, C. Lee, K. C. Min and N. S. Lee, Fourier transform Raman studies of methyl red adsorbed on γ-alumina and silica-alumina, *Bull. Korean Chem. Soc.*, 2014, **25**, 1817–1821.

32 P. Sejie and S. Nadiye-Tabbiruka, Removal of Methyl Orange (MO) from Water by adsorption onto Modified Local Clay (Kaolinite), *Phys. Chem.*, 2016, **6**, 39–48.

33 H. Wu, X. Dou, D. Deng, Y. Guan, L. Zhang and G. He, Decolourization of the azo dye Orange G in aqueous solution *via* a heterogeneous Fenton-like reaction catalysed by goethite, *Environ. Technol.*, 2012, **33**, 1545–1552.

34 M. K. Purkait, A. Maiti, S. DasGupta and S. De, Removal of congo red using activated carbon and its regeneration, *J. Hazard. Mater.*, 2007, **145**, 287–295.

35 Z. Ioannou, Ch. Karasavvidis, A. Dimirkou and V. Antoniadis, Adsorption of methylene blue and methyl red dyes from aqueous solutions onto modified zeolites, *Water Sci. Technol.*, 2013, **67**, 1129–1136.

36 T. Santhi, S. Manonmani and T. Smitha, Removal of methyl red from aqueous solution by activated carbon prepared from the Annona squmosa seed by adsorption, *Chem. Eng. Res. Bull.*, 2010, **14**, 11–18.

37 V. S. Munagapati, V. Yarramuthi and D.-S. Kim, Methyl orange removal from aqueous solution using goethite, chitosan beads and goethite impregnated with chitosan beads, *J. Mol. Liq.*, 2017, **240**, 329–339.

38 R. Lafi and A. Hafiane, Removal of methyl orange (MO) from aqueous solution using cationic surfactants modified coffee waste (MCWs), *J. Taiwan Inst. Chem. Eng.*, 2016, **58**, 424–433.

39 I. D. Mall, V. Srivastava and N. Agarwal, Removal of Orange-G and Methyl Violet dyes by adsorption onto bagasse fly ash – kinetic study and equilibrium isotherm analyses, *Dyes Pigm.*, 2006, **69**, 210–223.

40 A. Umar, M. M. Sanagi, A. A. Naim, W. N. W. Ibrahim, A. S. A. Keyon and W. A. W. Ibrahim, Removal of Orange G from Aqueous Solutions by Polystryene-Modified Chitin, *J. Teknol.*, 2017, **79**, 91–99.

41 P. Debye and E. Hückel Translated, The theory of electrolytes. I. Freezing point depression and related phenomenon, *Phys. Z.*, 2019, **1923**(24), 185–206.

42 A. Kundagrami and M. Muthukumar, Theory of Competitive Counterion Adsorption on Flexible Polyelectrolytes: Divalent Salts, *J. Chem. Phys.*, 2008, **128**, 244901.

43 J. C. Butler, T. Angelini, J. X. Tang and G. C. L. Wong, Ion Multivalence and Like-Charge Polyelectrolyte Attraction, *Phys. Rev. Lett.*, 2003, **91**, 028301.

44 B. K. Brettmann, N. Laugel, N. Hoffmann, P. Pincus and M. Tirrell, Bridging Contributions to Polyelectrolyte Brush Collapse in Multivalent Salt Solutions, *J. Polym. Sci., Part A: Polym. Chem.*, 2016, **54**, 284–291.

45 J. Yu, J. Mao, G. Yuan, S. Satija, W. Chen and M. Tirrell, The Effect of Multivalent Counterions to the Structure of Highly Dense Polystyrene Sulfonate Brushes, *Polymer*, 2016, **98**, 448–453.

46 U. T. D. Huynh, A. Lerbret, F. Neiers, O. Chambin and A. Assifaoui, Binding of Divalent Cations to Polygalacturonate: A Mechanism Driven by the Hydration Water, *J. Phys. Chem. B*, 2016, **120**, 1021–1032.

47 T. T. Nguyen, A. Y. Grosberg and B. I. Shklovskii, Screening of a Charged Particle by Multivalent Counterions in Salty Water: Strong Charge Inversion, *J. Chem. Phys.*, 2000, **113**, 1110–1125.

48 K. Besteman, K. Van Eijk and S. G. Lemay, Charge Inversion Accompanies DNA Condensation by Multivalent Ions, *Nat. Phys.*, 2007, **3**, 641–644.

49 M. Ghidiu, J. Halim, S. Kota, D. Bish, Y. Gogotsi and M. W. Barsoum, Ion-Exchange and Cation Solvation Reactions in Ti3C2 MXene, *Chem. Mater.*, 2016, **28**, 3507–3514.

50 S. Endo, A. Pfennigsdorff and K. U. Goss, Salting-Out Effect in Aqueous NaCl Solutions: Trends with Size and Polarity of Solute Molecules, *Environ. Sci. Technol.*, 2012, **46**, 1496–1503.

51 G. Sharma, E. Muthuswamy, M. Naguib, Y. Gogotsi, A. Navrotsky and D. Wu, Calorimetric Study of Alkali Metal Ion (K+, Na+, Li+) Exchange in a Clay-Like MXene, *J. Phys. Chem. C*, 2017, **121**, 15145–15153.

52 Y. Sun, Y. Sun, X. Meng, Y. Gao, Y. Dall'Agnese, G. Chen, C. Dall'Agnese and X. F. Wang, Eosin Y-sensitized partially oxidized Ti3C2 MXene for photocatalytic hydrogen evolution, *Catal. Sci. Technol.*, 2019, **9**, 310–315.